REYNOLDS AND MACH NUMBER SIMULATION OF APOLLO AND GEMINI RE-ENTRY AND COMPARISON WITH FLIGHT

By

B. J. Griffith and D. E. Boylan
ARO, Inc., Arnold Air Force Station, Tennessee

SUMMARY

A comprehensive investigation in the AEDC-VKF wind tunnels was conducted on the Apollo 011 and Gemini 3 spacecraft configurations in order to resolve several anomalies between preflight predictions and flight data. Attention was focused on simulating the actual Apollo Command Module (011) and Gemini spacecraft (GT3) "as flown" in model construction over a Mach number range of 3 to 20.

The investigation indicated that the influence of the ablator (heat shield) geometry of the Apollo Command Module causes a significant change in trim angle of attack and resulting decrease in available lift-to-drag ratio. In addition, a very strong viscous influence exists in the initial portion of re-entry for both the Apollo and Gemini spacecrafts. Also, the Mach number influence extends up to about Mach 14 which is substantially higher than previous blunt body investigations have indicated. Comparisons of the AEDC wind tunnel data with existing flight data are made and generally excellent agreement exists.

REYNOLDS AND MACH NUMBER SIMULATION OF APOLLO AND GEMINI RE-ENTRY AND COMPARISON WITH FLIGHT†

By

B. J. Griffith* and D. E. Boylan**
ARO, Inc., Arnold Air Force Station, Tennessee

1.0 INTRODUCTION

The motion of a spacecraft in flight is determined by the propulsive forces supplied, the force of gravity, the inertial characteristics of the spacecraft and the aerodynamic forces. The wind tunnel is generally recognized as being almost indispensable in obtaining the aerodynamic information necessary to define the motion of the spacecraft. However, the validity of wind tunnel data depends on the minimization of the possible sources of error and the simulation of the flow around the spacecraft in flight. The purpose of this paper is to present a direct comparison between flight and wind tunnel data from the Apollo Command Module and the Gemini Spacecraft during the re-entry phase. Attention is focused on (1) simulating Apollo spacecraft 011 (AS-202) and Gemini Spacecraft (GT3) "as flown" in model construction, (2) obtaining consistent pitch plane force measurements in the angle of attack range of interest, (3) defining the effect of Mach number over a range of 3 to 20 for the Apollo tests and 7 to 20 for the Gemini study, (4) defining the effect of Reynolds number, and (5) possible sting effects on the Apollo Command Module.

The aerodynamic model data reported herein were obtained in the 40-in. supersonic Tunnel A, the 50-in. hypersonic Tunnels B and C, the 100-in. hypersonic Tunnel F, the low-density hypersonic Tunnel L, and the hypervelocity Range G of the von Kármán Gas Dynamics Facility (VKF), Arnold Engineering Development Center (AEDC). Other Apollo and Gemini wind tunnel data utilized in this paper were taken from Refs. 1 and 2. The flight test results were obtained from Refs. 2 and 3. A more detailed documentation of the Gemini results is reported in Ref. 2.

2.0 FLIGHT TEST PROGRAM

Apollo mission AS-201 was flown on February 26, 1966 to demonstrate the structural integrity of the spacecraft (009) and to evaluate heat-shield performance during re-entry (see Ref. 4). The spacecraft was not fully instrumented for re-entry flight aerodynamic data. In addition, a failure in the reaction control system resulted in a positive rolling re-entry rather than the planned lifting re-entry. Therefore, spacecraft 009 was not simulated during the post flight investigation. Hence, no comparisons between flight and wind tunnel data are made in this paper.

Apollo mission AS-202 was flown on August 25, 1966. A pre-flight photograph of Spacecraft 011 (prior to flight AS-202) is shown in Fig. 1. A considerable amount of detailed aerodynamic re-entry data resulted from this flight (Ref. 3). Atmospheric data were obtained in the re-entry area. These measurements allowed a quantitative analysis between flight and pre-flight wind tunnel data to be made.

With one exception, comparison of pre-flight Apollo Command Module aerodynamic data and actual flight AS-202 data was good. The one anomoly which resulted was the decreased flight L/D ratio. Post-flight determination of the CM center of gravity confirmed the accurate determination of its location. The decreased flight L/D could then be traced to the fact that the vehicle trimmed at an angle of attack about 3.5 degrees more than pre-flight moment data indicated. The resulting error in L/D was one reason that a large uprange error (205 n.mile) in splash down position occurred.

The Gemini flight test data used in this paper were obtained during the re-entry phase of the GT2, GT3, GT4, and GT5 spacecrafts. The data were collected and analyzed by the McDonnell Aircraft Corporation for NASA. Additional information and data on these flights are given in Ref. 2.

3.0 WIND TUNNEL PROGRAM

3.1 BRIEF HISTORY OF APOLLO WIND TUNNEL PROGRAM (1962-1966)

The earlier Apollo wind-tunnel testing program (AWTTP), conducted prior to the present investigation, was established as part of the design and development program initiated in support of the Apollo spacecraft program. The AWTTP was designed

†Research reported in this paper was done at the request of the Arnold Engineering Development Center (AEDC), Air Force Systems Command (AFSC), under Program 920E in cooperation with the NASA Manned Spacecraft Center, Houston, Texas.

*Supervisor, Aerodynamics, Hypervelocity Branch, von Kármán Gas Dynamics Facility.

**Engineer, Aerophysics Branch, von Kármán Gas Dynamics Facility.

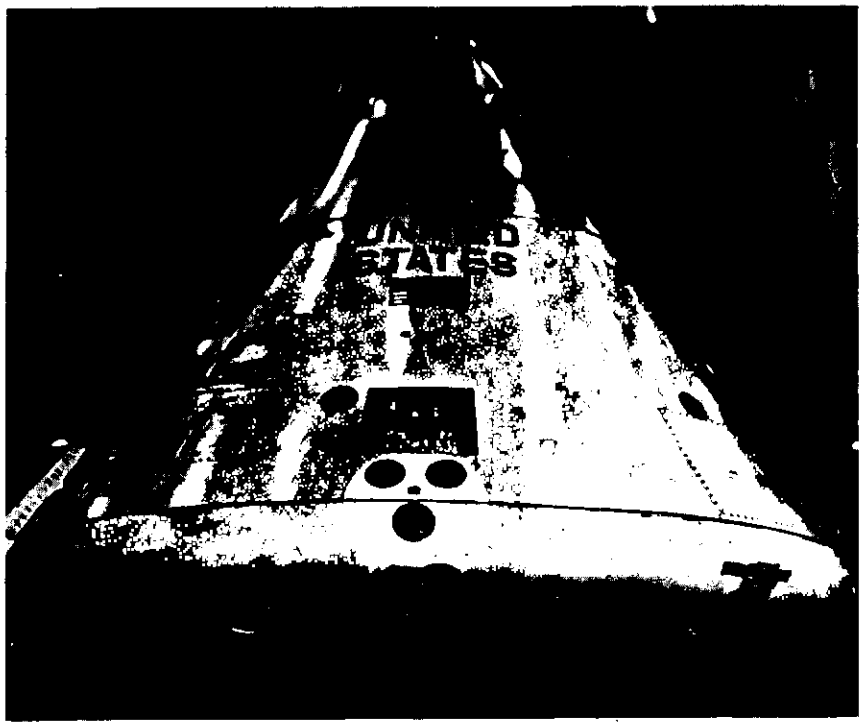

Fig. 1 Photograph of Apollo Spacecraft 011 Prior to Mission AS-202

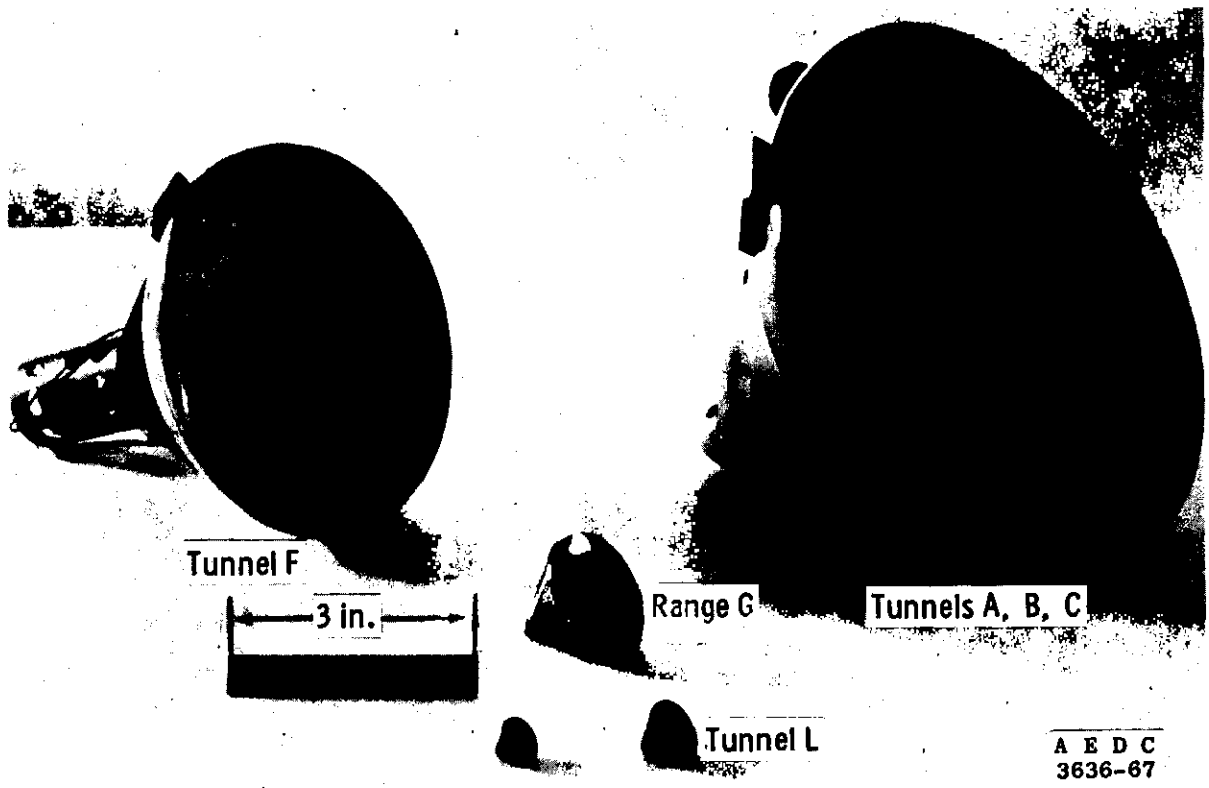

Fig. 2 Photograph of AEDC-VKF Apollo Models

to obtain the necessary aerodynamic data for detailed flight planning, flight analyses and abort trajectories to meet various mission requirements. The tests were conducted in 25 different tunnels having Mach number range capabilities from near 0 to Mach number 19. The program was the responsibility of North American Aviation as prime spacecraft contractor. Moseley and Martino (Ref. 5) have given an excellent comprehensive chronological summary of the wind tunnel test program. Moseley, Moore, and Hughes (Ref. 1) present stability characteristics of the Apollo Command Module. A detail summary of these two reports is beyond the scope of the present paper. Rather, attention is drawn only to the Apollo Command aerodynamics in the attitude of heat shield forward, i.e., the re-entry attitude.

The Command Module (CM) aerodynamics are important since the spacecraft is designed to employ a low L/D ratio for flight path control during re-entry into the earth's atmosphere. Since the CM will experience a wide variation of flow regimes from high altitude, high Mach number flight to low altitude, low Mach number flight; many different facilities were employed in an effort to provide the necessary flow regimes. Reference 5 includes a tabulation of the various wind tunnel facilities employed in the investigation of the Apollo CM aerodynamics. In addition, one low density free-flight wind tunnel test (Ref. 6) for which the heat shield was maintained in a forward attitude has been reported in the open literature. Primary parameters studied in these investigations were influence of model configuration, Mach number, and Reynolds number. Various studies have been devoted to the influence of sting mount and base pressure effects, heat shield geometry, and center of gravity location.

Static stability data were taken over a Mach number range of 0.20 to ~ 19. Tests were made using both the smooth command module and models with surface modifications. These modifications included antennas, umbilical fairing (including pad 5 fairing), vent protuberances, window and tower-leg cavities. However on flight AS-202, the 205 miles uprange landing was in some part due to the aerodynamic performance of the spacecraft. The flight lift-to-drag ratio was significantly less than predicted. The reasons have been determined to be: (1) The actual heat shield asymmetry and surface condition of spacecraft 011 were different from that used in the pre-flight wind tunnel program. All wind tunnel models tested during the AWTTP had smooth symmetrical heat shields. (2) The high Mach number data taken during the AWTTP were taken early in the program. Both the Cornell Aeronautical Lab. (CAL) Mach 15.8 data and the AEDC Mach 18.7 data were taken in 1962. The accuracy of these data was such that high Mach number effects could not clearly be defined.

3.2 POST-FLIGHT AEDC-VKF APOLLO (AS-202) WIND TUNNEL PROGRAM

A comprehensive wind tunnel program was undertaken in order to obtain additional wind tunnel data on the command module. Only the command module in the re-entry attitude was tested in order that a systematic and carefully analyzed wind tunnel program could be completed in a short period of time. The program was a correlated effort between NASA and AEDC. Attention was focused on (1) simulating the actual vehicle "as flown" in model construction, (2) obtaining consistent pitch plane force measurements in the angle-of-attack range $150 \leq \alpha \leq 180$ degrees, (3) the effect of Mach number over a range of 3 to 20, (4) the effect of Reynolds number, and (5) possible sting effects. Table 1 presents a brief description of the wind tunnel program and the AEDC-VKF test facilities utilized during the investigation. The first test was initiated in Tunnel L during the month of December, 1966. The final test entry was in Tunnel A during the month of May, 1967. A detailed listing of the test conditions is shown in Table 2.

A number of models were constructed for use in the correlation program. The models, shown in Fig. 2, ranged from 0.60 inches in diameter (heat shield) to 8.01 inches in diameter. For the Tunnel A, B, C, and F tests, the actual vehicle (spacecraft 011) "as flown" was simulated in model construction. Detail templates drawn to model scale were furnished to AEDC by the North American Aviation Company. These templates were computer fairings of actual vehicle measurements (spacecraft 011) after installation of the ablation material over the heat shield and afterbody. Pertinent details of the spacecraft ablation heat shield configuration are shown in Fig. 3. Added ablation material on the windward surfaces of the spacecraft produces an asymmetrical configuration. Ablation material over the pressure pads (supporting structure) makes the heat shield wavy. A view of the asymmetrical wavy heat shield model produced by the classical Toepler-Schlieren technique is shown in Fig. 4. To the authors' knowledge, no previous experimental investigation has been devoted to the asymmetrical wavy heat shield. Symmetrical heat shield models were also studied in the present investigation to provide consistent comparative data.

Pertinent model and sting details are presented in Fig. 5. The asymmetrical configurations were constructed according to templates to station $x/d = 0.30$ (see Fig. 5). Hence, the symmetrical and asymmetrical configurations are identical aft of this station. The asymmetrical model tested in the continuous tunnels included the umbilical housing and surviving antenna. The Tunnel F model included only the umbilical housing while the Tunnel L and Range G models had only symmetrical smooth

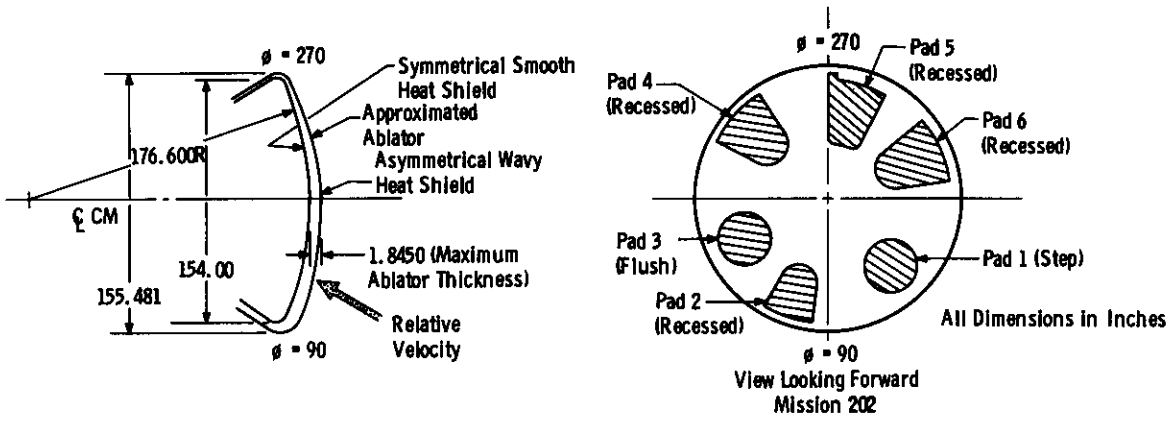

Fig. 3 Apollo 011 Heat Shield Asymmetry

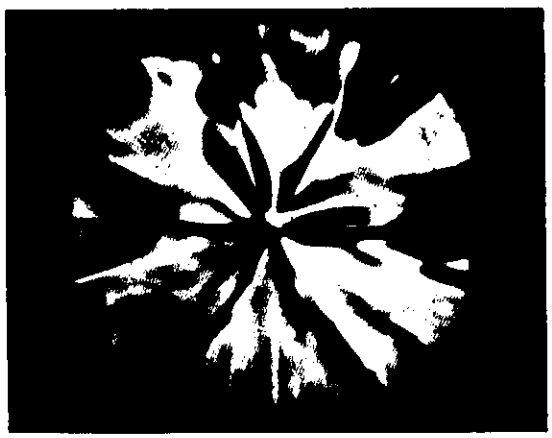

Asymmetrical Wavy Heat Shield

Fig. 4 Optical Photograph of Face of Tunnel F Model

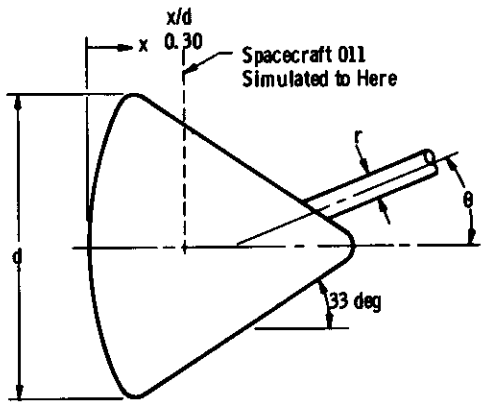

VKF Facility	d	θ, deg	r, in.	Asymmetrical Model
Tunnel A	8.01	20	1.65	Yes
Tunnel B	8.01	20	1.65	Yes
Tunnel C	8.01	20	1.65	Yes
Tunnel F	5.54	0	1.25	Yes
Range G	1.75	-	0	No
Tunnel L	0.60	0	0.16	No
	0.80	0	0.16	No

Fig. 5 Sketch of AEDC-VKF Apollo Models

heat shields and hence did not include any fairings. Details of these fairings are given in Ref. 3. The sign convention used for the Apollo data is given in Fig. 6.

3.3 AEDC-VKF GEMINI WIND TUNNEL PROGRAM

The AEDC-VKF wind tunnel program is documented by Griffith in Ref. 2. The program, although not as comprehensive as the Apollo study, presents a systematic study of the aerodynamics of the Gemini spacecraft in the re-entry attitude. Figure 7 presents the sign convention used for the Gemini data throughout the paper.

The Gemini investigation was conducted only in AEDC-VKF Tunnels F and L. The Tunnel F model was a 1/15-scale version of the Gemini re-entry module with detailed retaining strap fairings and observation windows. The Tunnel L models were 1/120- and 1/180-scale versions of the re-entry module and did not include fairings or observation windows. The reader is referred to Ref. 2 for additional details.

3.4 TEST FACILITIES FOR CURRENT INVESTIGATION

The Apollo investigation was conducted in the 40-in. supersonic tunnel (Gas Dynamic Wind Tunnel, Supersonic (A)), in the 50-in. hypersonic tunnel (Gas Dynamic Wind Tunnel, Hypersonic (B)), the 50-in. Mach 12 tunnel (Gas Dynamic Wind Tunnel, Hypersonic (C)), the 100-in. Mach 20 tunnel (Gas Dynamic Wind Tunnel, Hypersonic (L)), and the 1000-ft. Hypervelocity Range (G). Only Tunnels F and L were utilized during the Gemini investigation.

Tunnel A is a continuous, closed-circuit, variable-density, supersonic wind tunnel with a Mach number range of 1.5 to 6. The tunnel operates at stagnation pressures between 1.5 to 200 psia and stagnation temperatures of 70 to 290°F.

Tunnel B (a continuous closed-circuit wind tunnel) operates at a nominal Mach number of 6 or 8 at stagnation pressures from 20 to 280 or from 50 to 900 psia, respectively, at stagnation temperatures up to 890°F.

Tunnel C (similar to Tunnel B) operates at a nominal Mach number of 10 or 12 at stagnation pressures from 200 to 2000 or from 600 to 2400 psia, respectively, at stagnation temperatures up to 1440°F. The data presented in this paper at Mach 12 represent the first test (except for calibration) in the Mach 12 nozzle.

Tunnel F is an arc-driven wind tunnel with a 100-in. test section. Nitrogen, initially confined in an arc chamber by a diaphragm located near the throat of an attached 8-deg conical nozzle, is heated and compressed by an electric arc discharge and expanded through the conical nozzle to the test section. A useful run time between 50 and 100 msec is attained.

Tunnel L is a low-density, hypersonic, continuous-flow, arc heated, ejector-pumped facility, normally using nitrogen or argon as the test gas. Nitrogen was used for all the tests reported herein. Contoured nozzles provide gradient free flow at nominal Mach numbers of 4, 9, and 10 at varying free-stream Reynolds numbers.

Hypervelocity Range G is a 1000-ft-long, 10-ft-diameter, variable density tube wholly contained within an underground tunnel. Launching capability ranges from in-gun weights of 498 gms at 12,000 ft/sec to 130 gms at 23,000 ft/sec. Instrumentation includes provisions for pressure and temperature measurements, forty-three dual-axis shadowgraph stations, schlieren photography, microwave and RF cavity measurements, radiometric and spectrographic measurements, and high speed photography.

3.5 PROCEDURE

The broad range of flight conditions during Apollo flight AS-202 demanded that several of the AEDC-VKF tunnels be utilized. In order to keep the experimental program to a minimum, the results of a given test entry were analyzed before the next test was started. For example, tests in Tunnel L were started prior to the Tunnel F tests in order to determine the viscous influence at simulated altitudes up to 350,000 ft. These tests resulted in a more meaningful experimental program in Tunnel F. However, the post-flight tests still required 515 hours of testing. The same general procedure was followed during the Gemini studies. A summary of the Apollo testing program is as follows:

1. Viscous Effects at High Simulated Altitudes

Tests were conducted in Tunnel L at Mach numbers of 9.37 and 10.15. The free-stream Reynolds number (based on heat sheild diameter) ranged between 234 and 1283 by varying test conditions and model size. These tests were conducted during the period of 5 December 1966 to 9 January 1967.

2. Viscous and Mach Number Effects at Simulated Altitudes of 220,000 to 280,000 ft, Plus A Study of the Influence of the Ablator (Heat Shield Geometry)

These tests were conducted during the period of 26 December 1966 to 24 January 1967 in Tunnel F. Data were obtained over a Mach number range of 14.6 to 20 at free-stream Reynolds numbers of 13,700 to 377,000.

3. Viscous and Mach Number Effects at Simulated Altitudes of 150,000 to 200,000 ft, Plus A Study of the Influence of the Ablator (Heat Shield Geometry)

The first tests were conducted at Mach 8 in Tunnel B over a Reynolds number range ($Re_{\infty,d}$) of 0.36×10^6 to 1.8×10^6 on 17 January 1967. The tests were conducted using a small (amplitude (±3 deg), free oscillation, cross-flexure pivot balance in order to better define the trim angle. The data indicated the need for force coefficients at similar conditions. Additional tests were conducted on 23 February 1967 with a six-component, force-type, strain-gage balance.

4. Additional Data in the High Mach Number, Low Reynolds Number Range

Additional data were obtained in Tunnel F during the week of 15 February 1967 in order to better define the variation of the Apollo force and moment coefficients with Reynolds number.

5. Verification of the Apparent Mach Number Effect

Tests were conducted in Tunnel A on 18 May 1967 at Mach 3, 4, and 6 and on 26 May 1967 in Tunnel C at Mach 12. These data were necessary in order to better define the effect of Mach number on the force and moment coefficients of the Command Module.

6. Sting Effects

Concurrent with the tests on the sting mounted models, configurations with the symmetrical smooth heat shield were being launched in Range G in order to study any possible influence of the sting. Shots were made with models that had full CG offsets (same as spacecraft AS-202), half offsets and zero offsets. The shots were made as near as possible to the Tunnel B test conditions and were made from 25 January 1967 to 25 March 1967.

3.5 ACCURACY AND REPEATABILITY

The accuracy of the data is, of course, a function not only of the uncertainty of the direct measurements but also of the test-section flow properties. Except for the Mach 6 data in Tunnel A the test-section static temperature was kept within a few degrees of the theoretical liquefaction value in order to add validity to the calculated flow properties. Assessments of the estimated uncertainties in the Apollo tunnel and Range data are as follows:

	C_A	C_D	C_N	$C_{m_{cg}}$	α_T
Tunnel A	±0.01	±0.01	±0.002	±0.0012	- - -
Tunnel F	±0.01	±0.01	±0.002	±0.0012	- - -
Tunnel C	±0.01	±0.01	±0.002	±0.0012	- - -
Tunnel F	±0.04	±0.04	±0.005	±0.0018	- - -
Tunnel L	±0.03	±0.03	±0.02	±0.0025	- - -
Range G	- -	±0.01	- -	- - -	±1.2 deg

The estimated uncertainties for the Gemini wind tunnel data are similar to the above and are given in Ref. 2.

4.0 WIND TUNNEL CORRELATION PARAMETER

The comparison of wind tunnel or range data with flight data requires the determination of a suitable correlation parameter. The need for a correlation parameter, of course, is due to the fact that flight conditions can seldom be duplicated in the wind tunnel. Figure 8 shows the re-entry of Apollo 011 and Gemini 3 in terms of altitude and time. However, Fig. 9 gives (for the same flights) the normal shock stagnation conditions necessary for flight duplication.

Viscous effects are sometimes scaled using free-stream Reynolds number as the scaling parameter, but it is well known that this is not always the best procedure. Higher altitude viscous interaction effects have been successfully accounted for using the parameter $\bar{v}_\infty$ (Ref. 7). Both a Re_∞ and $\bar{v}_\infty$ parameter appear to be applicable to either blunt or sharp slender bodies or for configurations for which viscous effects are of second order importance. However, the flow field of interest about

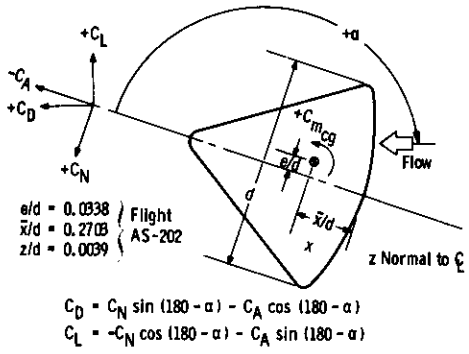

Fig. 6 Apollo Spacecraft 011 - Orientation of Forces and Moments

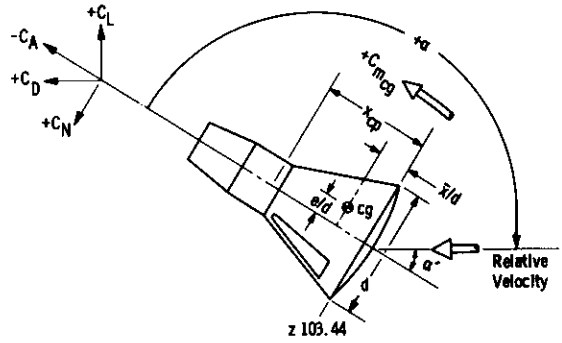

Fig. 7 Gemini 3 Spacecraft - Orientation of Forces and Moments

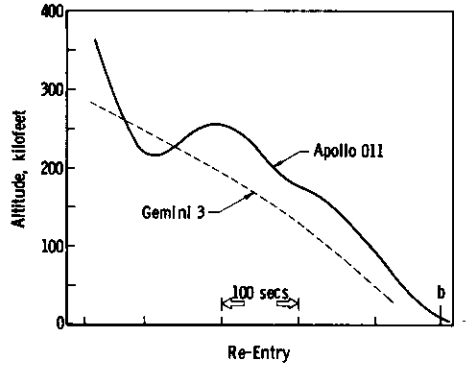

Fig. 8 Re-Entry Trajectory of Apollo 011 and Gemini 3

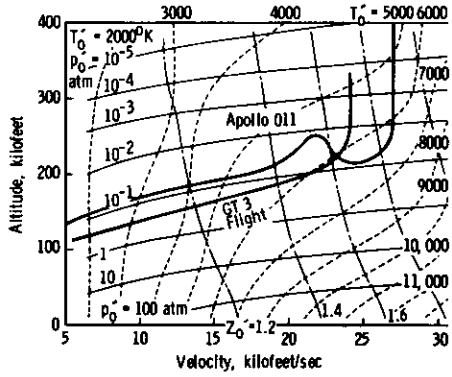

Fig. 9 Normal Shock Stagnation Conditions at Flight Duplication

a very blunt body such as the Apollo CM is the flow which is separated from the free-stream by the bow shock wave.

If the bow shock is strong everywhere ($M_\infty \sin \theta_b \gg 1$), the density ratio ϵ approaches the limit $(\gamma-1)/(\gamma+1)$ and the flow quantities immediately behind the shock become dependent upon only ρ_∞, U_∞, and σ.* In addition, the local Mach number M_2 is always a low subsonic value with only about a 2 percent variation between M_∞ = 10 and 25. The shock Reynolds number Re_{2d} may be expressed as

$$Re_{2d} = \rho_2 U_2 d/\mu_2$$
$$= (\rho_\infty U_\infty d)/\mu_2$$

where d is the characteristic length chosen as the diameter of the heat shield in the present case.

An improved parameter would be one which would account for wall temperature effects (Ref. 8) such as:

$$Re_{wd} = (Re_{2d})\mu_2/\mu_w$$

However, lack of adequate wind tunnel and flight wall temperature values and the fact that

$$\mu_\infty/\mu_2)_{\text{wind tunnel}} \cong \mu_\infty/\mu_2)_{\text{flight}}$$

in the present case suggests that Re_{2d} should be an adequate correlation parameter between flight and wind tunnel data as long as the free-stream Mach number is high. However, the present data show that the Apollo Command Module aerodynamics are sensitive to variations in free-stream Mach number below a value of approximately fourteen. The data also indicate that above a Re_{2d} value of about 10^4 the aerodynamics of the module are insensitive to further increases in Reynolds number.

Flight values of Re_{2d} for Apollo mission AS-202 are shown in Fig. 10. The velocity profile from the flight data was used in conjunction with the 1962 standard atmosphere and the viscosity values of Ref. 9 and Ref. 10 for the calculation of Re_{2d}. Calculations based on flight values of free-stream pressure and temperature gave essentially the same results. For the flight data, real gas normal shock relationships from Lewis and Burgess (Ref. 10) were employed. VKF wind tunnel data reduction programs include calculation of shock Reynolds number. Nominal facility test conditions (for Apollo) obtained during the present investigation are indicated in Fig. 10 and tabulated in Table 2 to illustrate the regions of flight simulation achieved. Figure 11 compares both the Mach number (M_∞) and Reynolds number variation (Re_{2d}) of mission AS-202 with the facility test conditions. Note that although a variation of nearly five orders of magnitude in Reynolds number is shown, actual Mach number and Reynolds number simulation are achieved only at M_∞ = 6 and 8. However, it will be shown that this lack of simulation, although undesirable, is not serious.

The basis of the correlation presented in this report (for the Apollo) is illustrated in Fig. 12. When the pitching-moment data from the present investigation at a given angle of attack are plotted versus Re_{2d}, a consistent trend at values of Re_{2d} above 10^4 does not exist. However, plotting the same data ($Re_{2d} > 10^4$) versus Mach number presents a consistent variation. The other aerodynamic data (C_N, C_A) on the Apollo CM exhibit similar trends. The wind tunnel data at values of $Re_{2d} <$ 200 were at Mach numbers of 9.4 and 10.2 (see Fig. 11). However, the strong viscous effects in this regime should make variations in free-stream Mach number rather insignificant.

The lack of a comprehensive set of wind tunnel data on the Gemini configuration prevented a similar type correlation. To circumvent this problem, approximate inviscid values of C_N and center of pressure ($X_{c.p.}$) where obtained by extrapolation of existing data. The reader is referred to Ref. 2 for additional details and information on the correlation procedure used for the Gemini data.

5.0 WIND TUNNEL DATA CORRELATION

The AEDC-VKF data are correlated over a free-stream Reynolds number range of 234 to 1.9 x 10^6 based on heat shield diameter and a Mach number range of 2.98 to approximately 20. Typical basic data are shown in Fig. 13. The resulting correlations are shown in Figs. 14 through 16. The data points presented represent fairings of the basic data.

*Neglects effects of shock and boundary layer merging at the higher simulated altitudes.

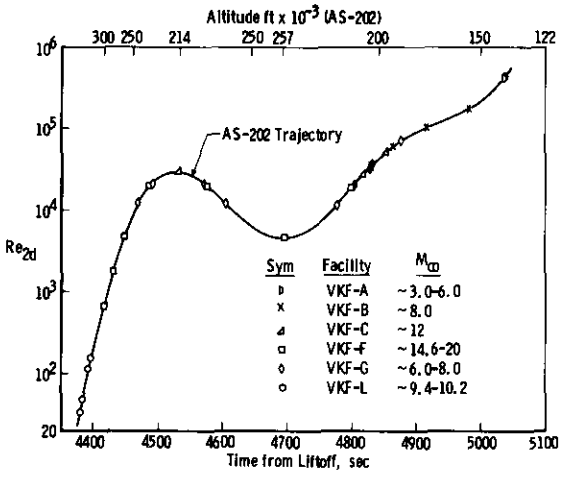

Fig. 10 Shock Reynolds Number Flight Simulation, Apollo

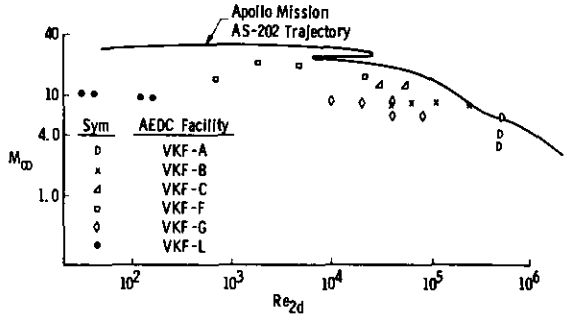

Fig. 11 Mach Number and Shock Reynolds Number Flight Simulation, Apollo

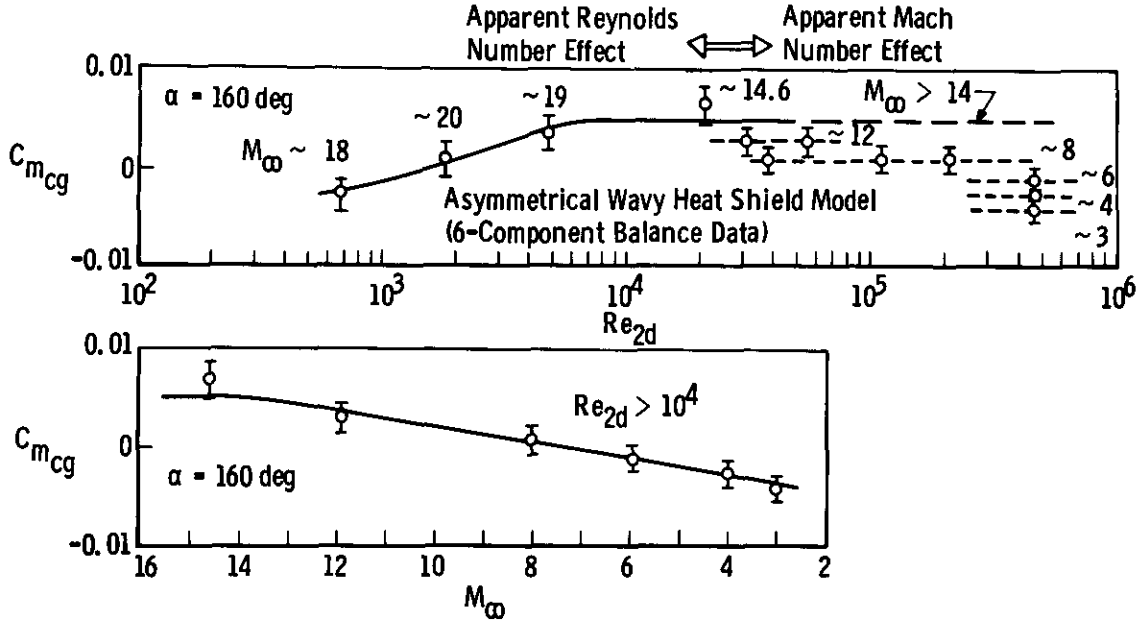

Fig. 12 Typical Data Plot Showing Basis of Data Correlation, Apollo

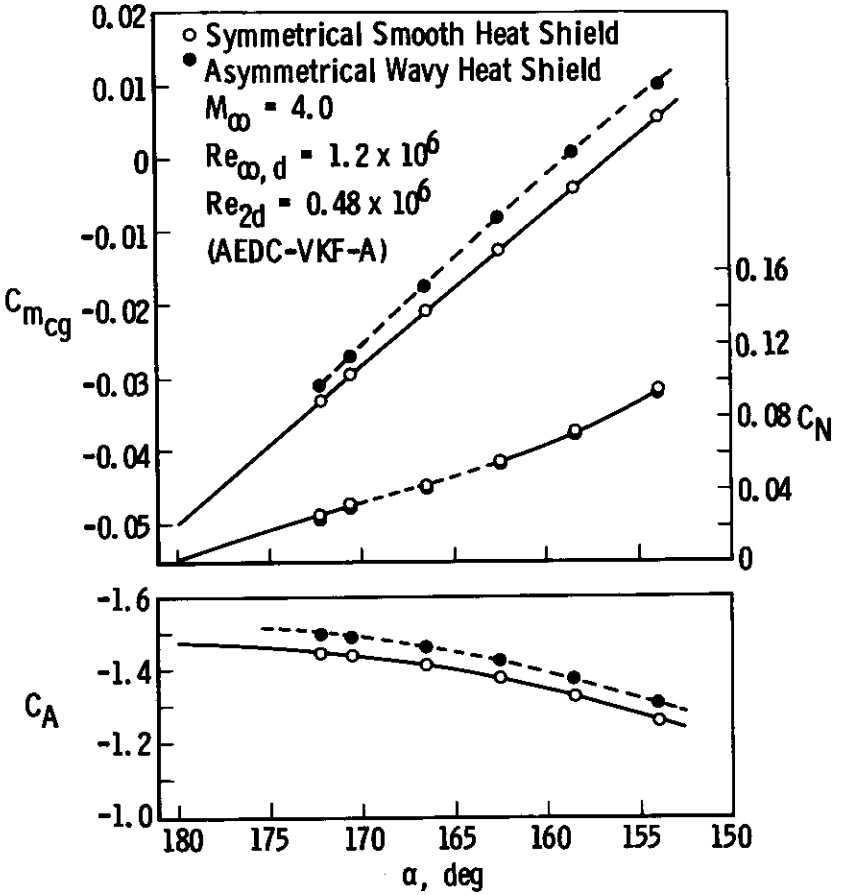

a. Multi-Component Balance Data, M_∞ = 4

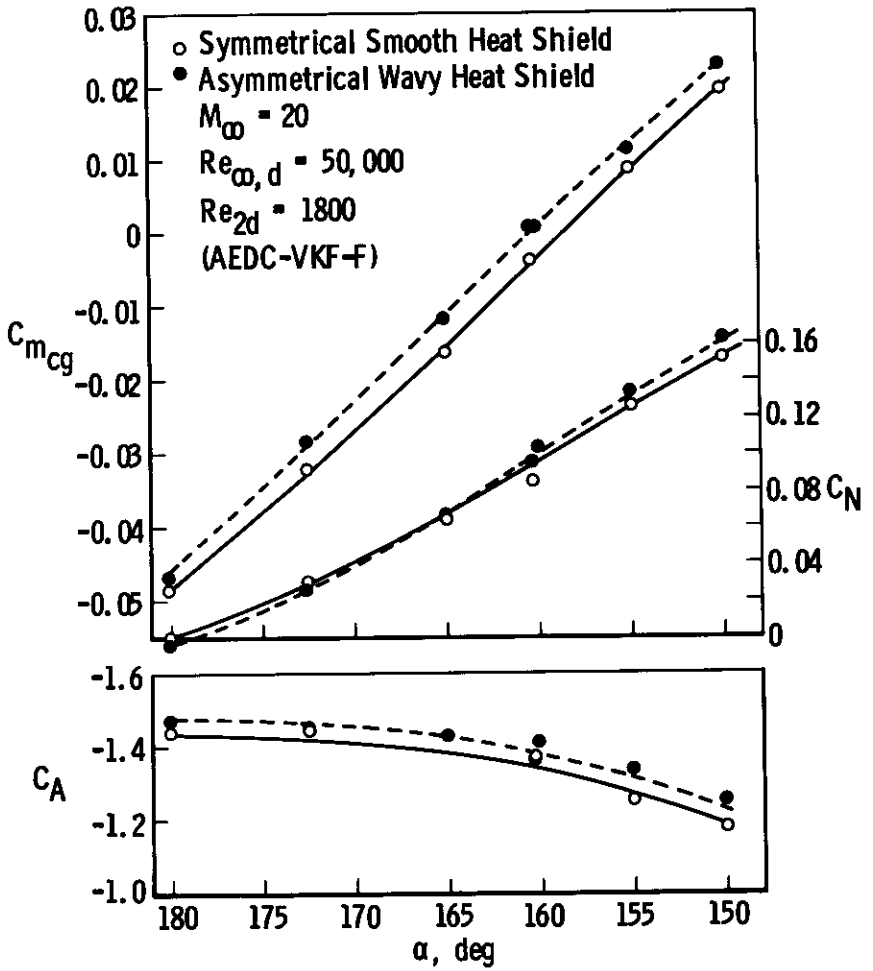

b. Multi-Component Balance Data, M_∞ = 20

Fig. 13 Typical Basic Data, Apollo

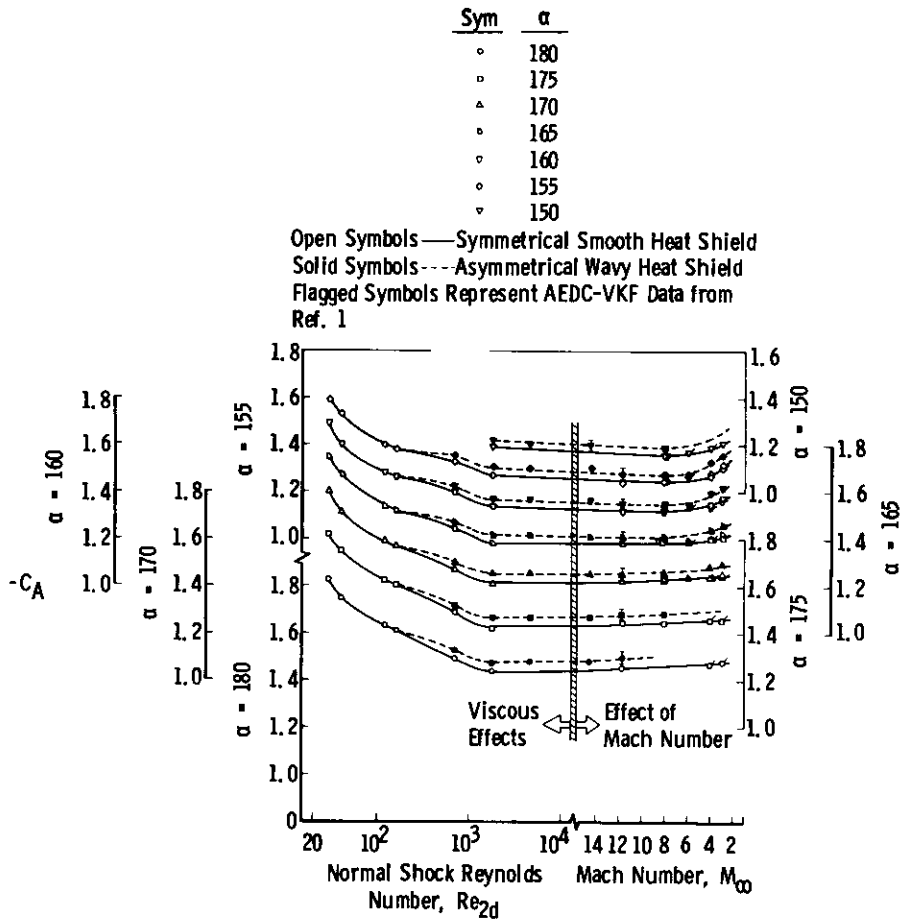

Fig. 14 Variation of Axial-Force Coefficient (C_A) with M_∞ and Re_{2d}, Apollo

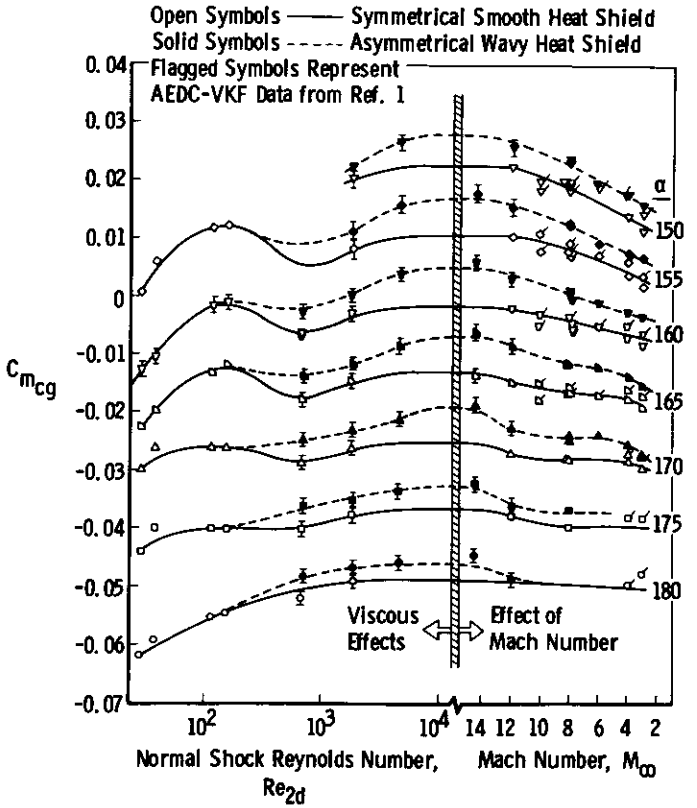

Fig. 15 Variation of Pitching-Moment Coefficient ($C_{m_{cg}}$) with M_∞ and Re_{2d}, Apollo

Figure 14 shows the variation of the axial force coefficient of the Apollo CM with Re_{2d} and Mach number. Note the significant increase in C_A at values of Re_{2d} below 1000 and the slight increase at the lower free-stream Mach numbers. The reference area of the symmetrical smooth heat shield is used in data reduction which, in part, accounts for the higher axial force of the asymmetrical wavy heat shield configuration. Model scale limitations did not permit the asymmetrical wavy heat shield to be studied at low values of Re_{2d}. Therefore, the aerodynamics of the symmetrical and asymmetrical models are assumed to be identical below a Re_{2d} of 200 since viscous effects should dominate in this flow regime.

Significant variations in the pitching moment ($C_{m_{cg}}$) of the Apollo CM with Reynolds number, Mach number and heat shield configuration are shown in Fig. 15. The effect of the asymmetrical wavy heat shield is greater at the high Mach number-high Reynolds number flight condition ($M_\infty \geq 14$ and $Re_{2d} \geq 5000$) which represents a major portion of Apollo flight AS-202. Additional data in this important test regime would have been helpful.

The normal force coefficient (C_N) is presented in Fig. 16. Viscous effects are significant below a Re_{2d} value of about 7000 whereas variations of C_N due to Mach number are generally slight. The asymmetrical wavy heat shield causes a decrease in the normal force (C_N) only at angles of attack between 170 and 180 degrees.

The lack of a comprehensive set of wind tunnel data on the Gemini configuration prevented an analysis identical to the Apollo. However, a systematic analysis was possible by working with the center of pressure ($X_{c.p.}$) instead of the moment coefficient $C_{m_{cg}}$. A summary of the C_N and $X_{c.p.}$ correlation versus Re_{2d} is presented in Fig. 17. Note the near order-of-magnitude decrease in C_N between the lower Re_{2d} data and the predicted inviscid level; note also the sudden rearward shift in center of pressure when Re_{2d} was increased from 2400 and 5400. The Apollo data will exhibit a similar trend if plotted in the same manner.

6.0 RESULTS AND DISCUSSION

6.1 APOLLO SPACECRAFT FLIGHT-WIND TUNNEL COMPARISONS

A comparison between the Apollo AS-202 flight trim angle of attack and wind tunnel data is presented in Fig. 18. Note the good agreement of the asymmetrical wavy model wind tunnel data with the flight test data over the regime of trimmed flight. The correlation was made by using Re_{2d} as the correlation parameter from re-entry to an altitude (177,000 ft) at which $M_\infty = 14$ was reached and a Mach number correlation below this altitude. The correlation curves were obtained by cross plots of Fig. 15. The flight test data were obtained from the paper by Hillje (Ref. 3). The post-flight symmetrical model correlation along with the pre-flight estimate (Ref. 3) are given for completeness. The pre-flight estimate was based on previous symmetrical model data. A summary of the ligt-to-drag ratios (L/D) for Flight AS-202 is shown in Fig. 19. Again, good agreement is noted between the flight and asymmetrical wavy model wind tunnel data. The offset CG of spacecraft 011 changes during the final re-entry phase due, in part, to fuel usage. The effect of this variation on the correlated wind tunnel data is also shown in Figs. 18 and 19.

Figure 20 compares the present trim angle of attack and corresponding L/D to Apollo Mission AS-202 flight data. However, the comparative data are shown as functions of Re_2 and M_∞ rather than flight time, as used in Figs. 18 and 19, to illustrate the strong viscous influences found in the present study. The strong viscous influence found in the present study is also illustrated in Fig. 21.

In order to determine if the wind tunnel data were free of significant sting effects, several models were launched in the 1000-ft Range G at AEDC-VKF. A comparison of the free-flight Range G data with the wind tunnel data is shown in Fig. 22. Note the good agreement and apparent lack of sting effects.

6.2 GEMINI SPACECRAFT FLIGHT-WIND TUNNEL COMPARISONS

The comparison between the Gemini 3 flight test data and the AEDC-VKF wind tunnel data is shown in Fig. 23. Excellent agreement is noted between the two sets of data. The increase in the predicted trim angle-of-attack curve that occurs near an altitude of 240,000 ft is caused by the center-of-pressure shift shown in Fig. 17. The Gemini 3 flight data do not indicate the increase; however, flight data from GT2 and GT4 give some indication that the shift in center of pressure exists (see Ref. 2). Langley Mach 6.89 data (Ref. 2) are also in excellent agreement with GT3 flight data. The Langley data are correlated on a Mach number basis since insufficient data were available for correlating this lower Mach number with the high Mach number correlation of Fig. 17. A summary of the lift-to-drag ratios versus angle-of-attack for two flight regimes is given in Fig. 25. The Gemini flight and Tunnel F data are in excellent agreement.

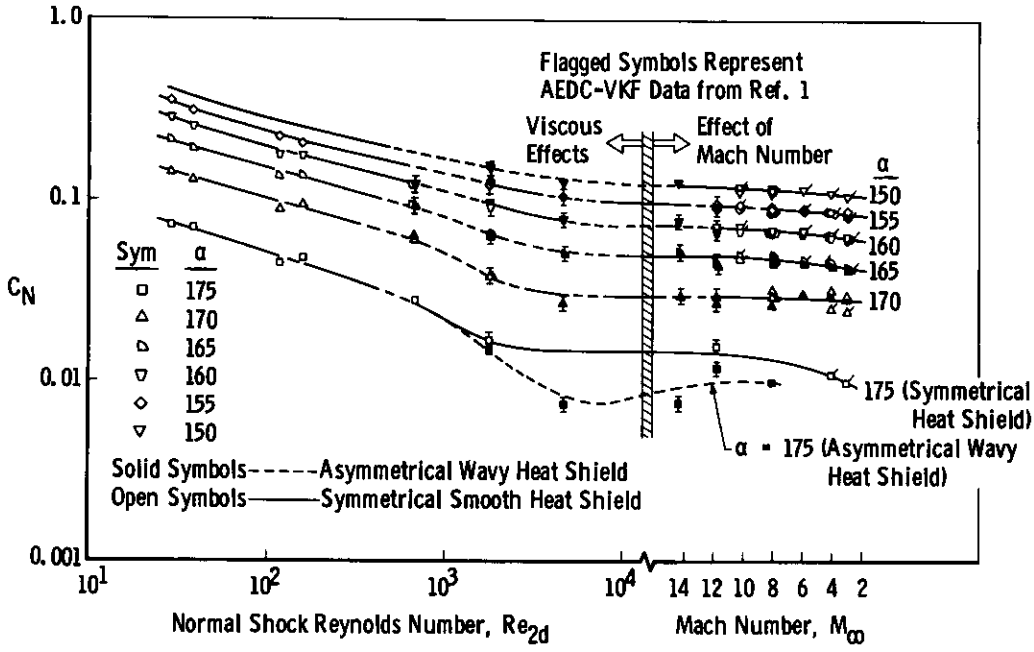

Fig. 16 Variation of Normal-Force Coefficient (C_N) with M_∞ and Re_{2d}, Apollo

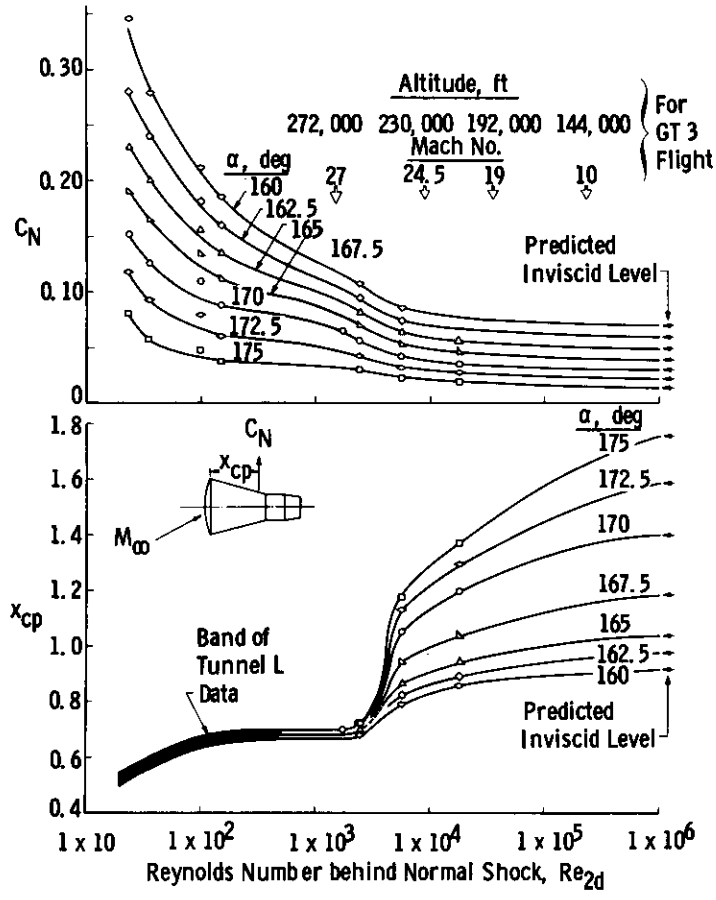

Fig. 17 Correlated Wind Tunnel Data on Gemini

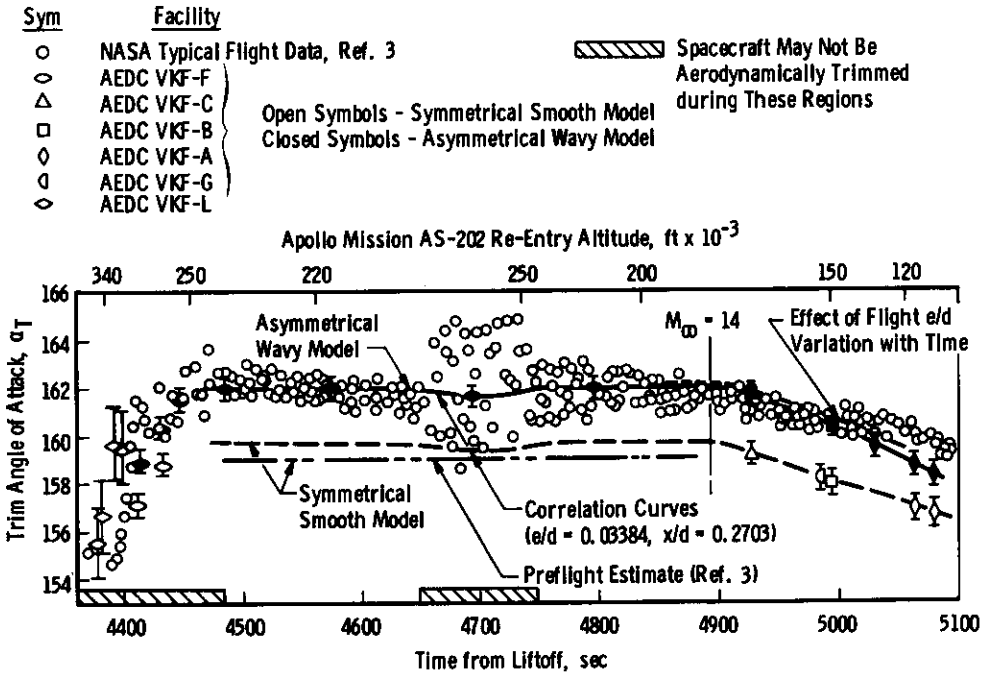

Fig. 18 Comparison of Mission AS-202 Trim Angle of Attack with AEDC-VKF Tunnel Data

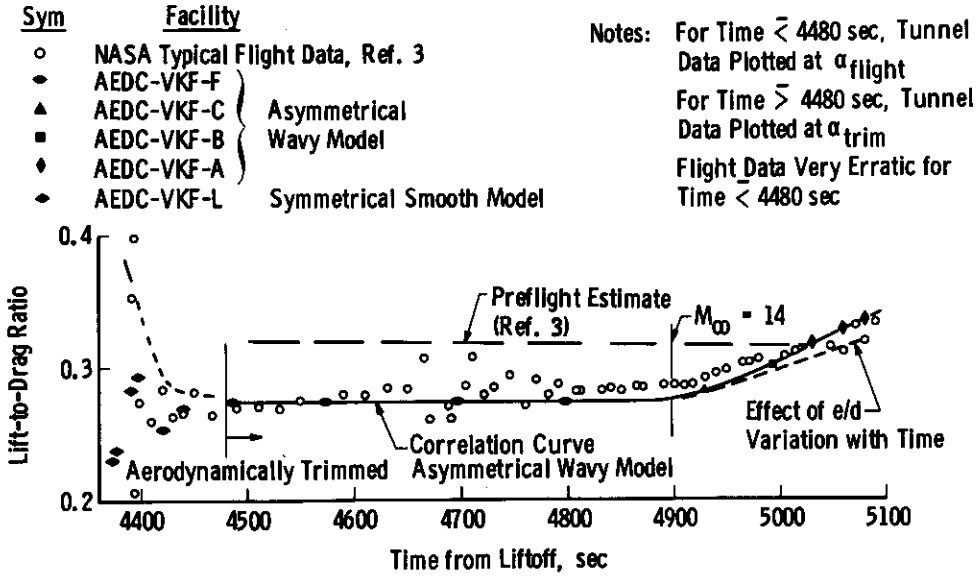

Fig. 19 Comparison of Mission AS-202 Lift-to-Drag Ratio with AEDC-VKF Tunnel Data, Apollo

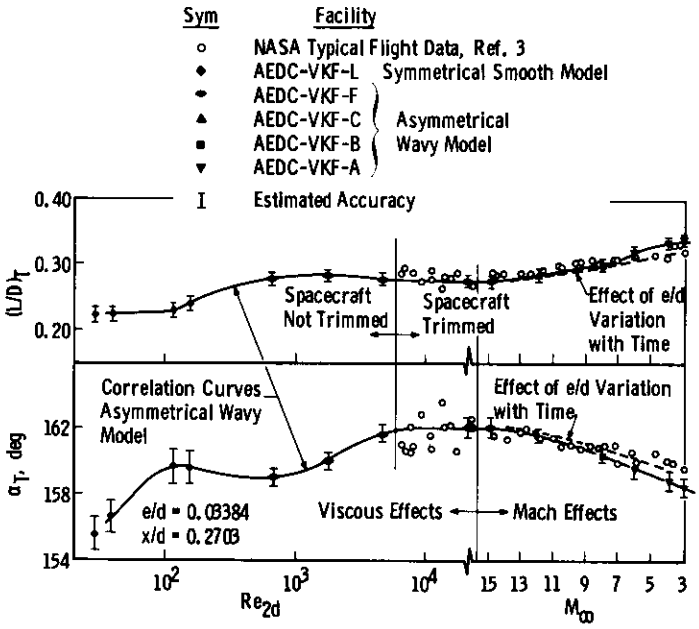

Fig. 20 Summary of Apollo L/D and α_T Data

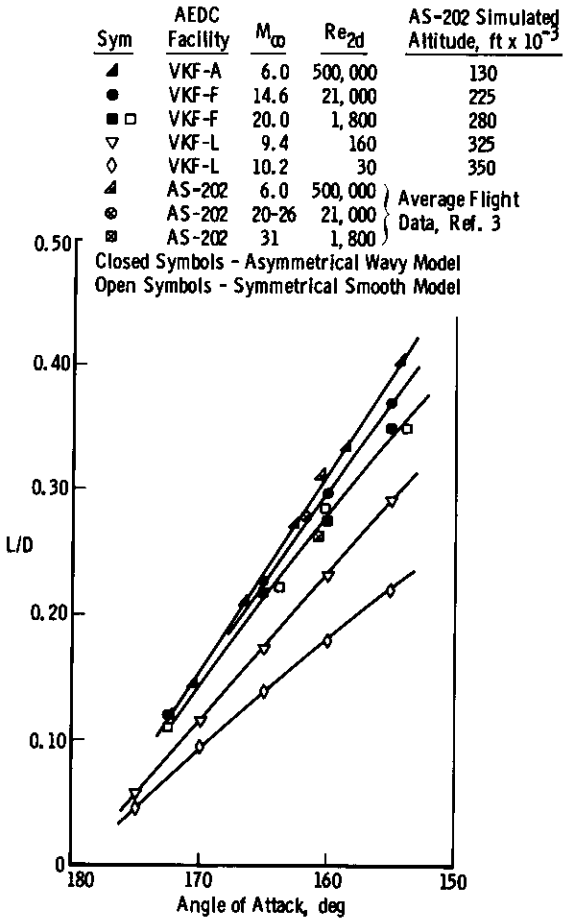

Fig. 21 Effect of Mach Number and Shock Reynolds Number on Lift-to-Drag Ratio, Apollo

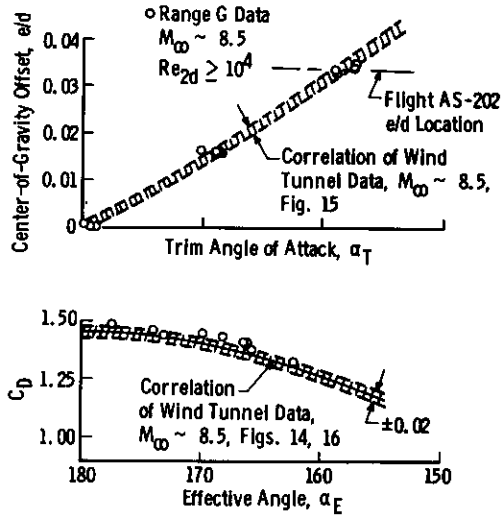

Fig. 22 Comparison of Free-Flight (AEDC-Range G) to Sting Mounted Tunnel Data

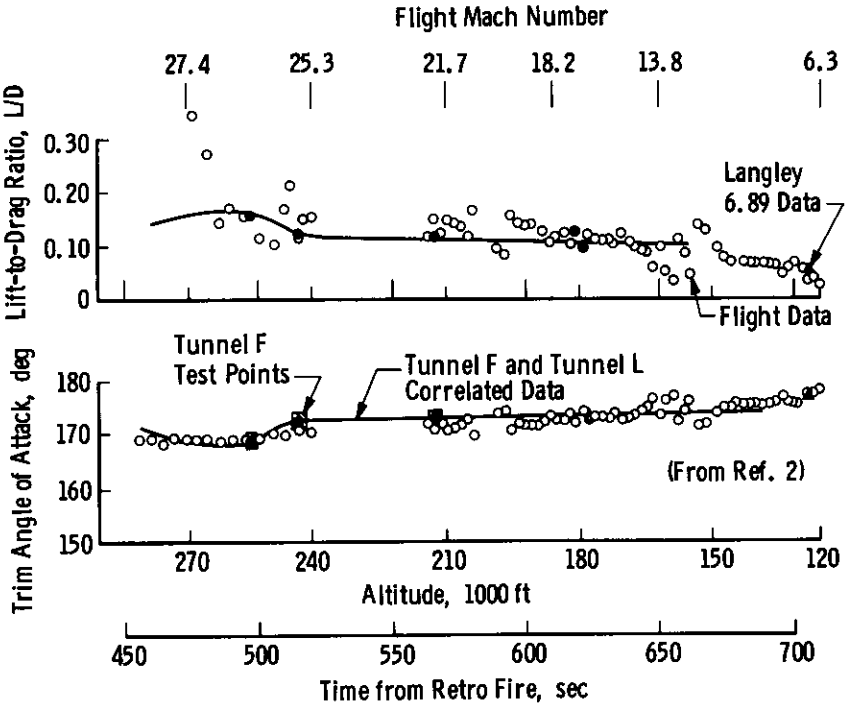

Fig. 23 Comparison of Gemini 3 Flight Data with AEDC and Langley Wind Tunnel Data

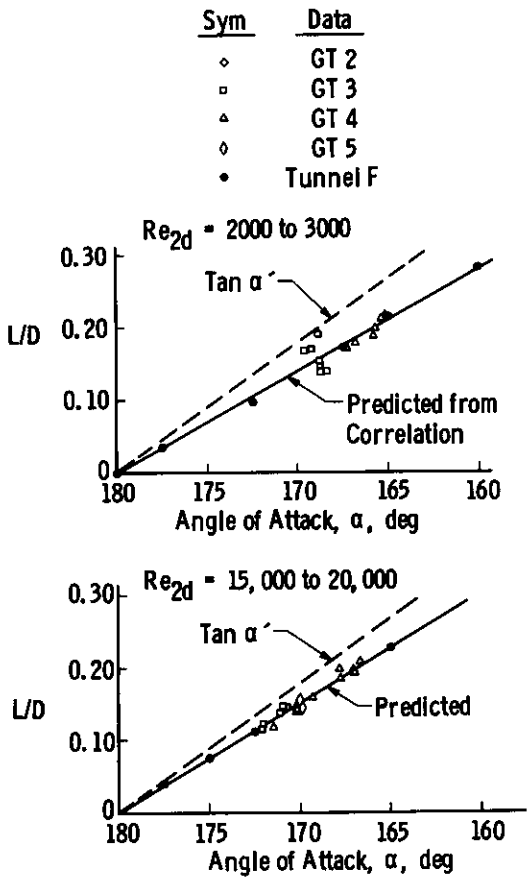

Fig. 24 Comparison of Flight and Tunnel F Lift-to-Drag Ratios for the Gemini

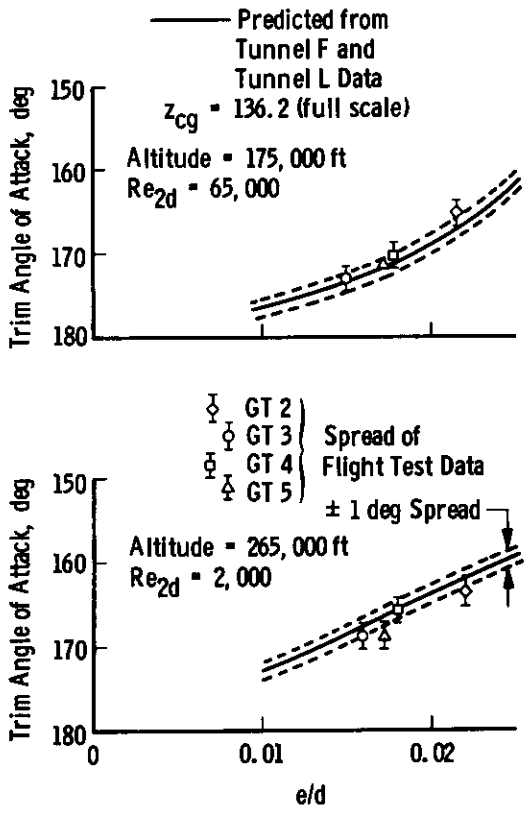

Fig. 25 Comparison of Flight and Wind Tunnel Data for Various Values of e/d

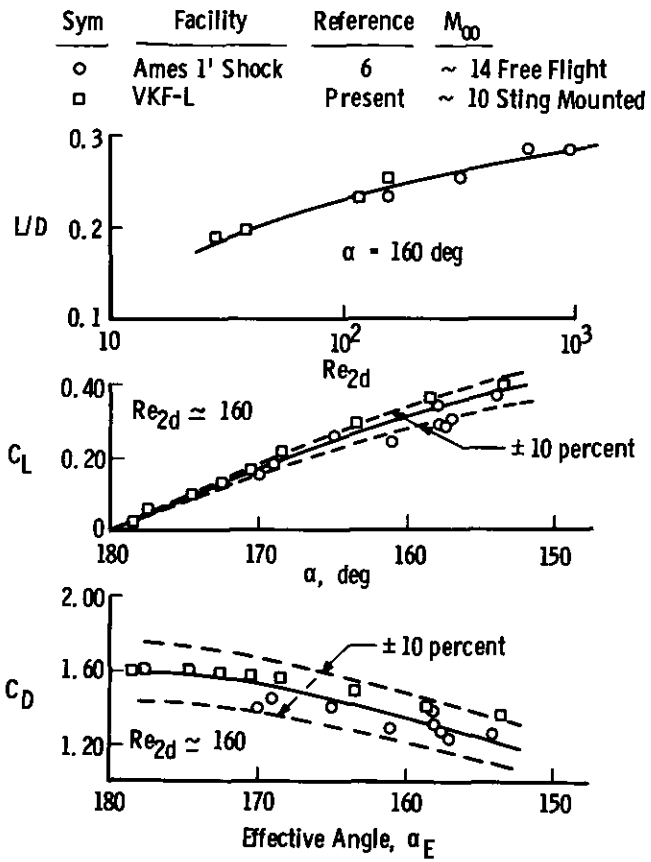

Fig. 26 Comparison of Free-Flight (Ames Shock Tunnel) to Sting Mounted Tunnel Data

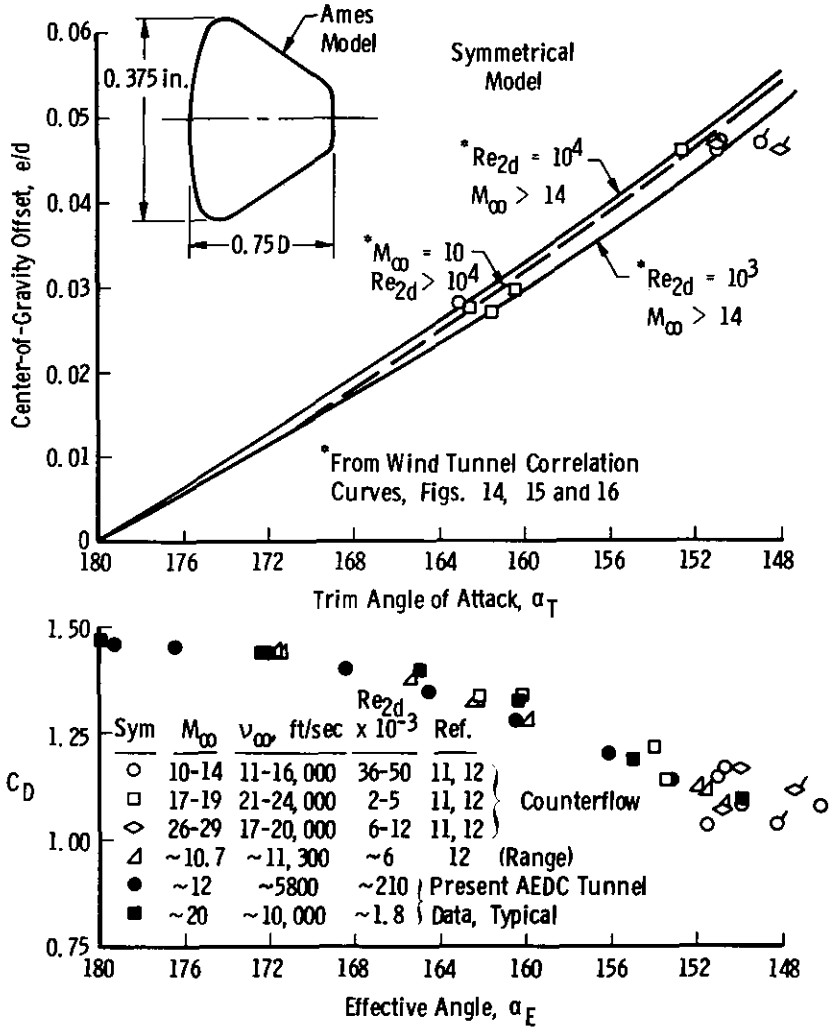

Fig. 27 Comparison of Ames Free-Flight (Counterflow) and AEDC Wind Tunnel Data

The flight test trim angles are plotted in Fig. 25 versus the cg offset (e/d) associated with a number of flights. The data are shown for Re_{2d} values of 2000 and 65,000 and indicate the consistency of the flight results. The trim angle for GT5 at the lower value of Re_{2d} is noted to be somewhat low when compared to the other flights.

6.3 COMPARISON OF AMES FREE-FLIGHT DATA AND AEDC WIND TUNNEL DATA

The low density free-flight data of Horstmann and Kussoy (Ref. 6) from the Ames 1-ft shock tunnel are compared to the AEDC-VKF Tunnel L sting mount data in Fig. 26. Again, as noted in Fig. 24 for the higher density VKF-Range G data, no apparent effect of the support sting is noted.

To investigate the effect of velocity, Mach number, and Reynolds number, DeRose (Ref. 11) measured the trim angle and drag coefficient of Apollo Command Module at speeds up to 24,000 ft/sec in the Ames Counterflow facilities (also see Ref. 12). These data are compared with the AEDC-VKF wind tunnel data in Fig. 27. No apparent effect of velocity, Mach number or Reynolds number is noted. Also general agreement with the AEDC-VKF data is noted, again indicating no apparent sting effects in the AEDC data. An average of the Ames data (at $e/d \sim 0.046$) would indicate a slightly lower trim angle than the tunnel data. The shortened version of the Apollo Command Module used in the Ames tests would have a tendency to produce this trend in the data.

7.0 CONCLUDING REMARKS

Post-flight investigations were undertaken in order to obtain static stability characterisitcs of the Apollo Command Module "as flown" during flight AS-202 and the Gemini 3 spacecraft. The principle conclusions of the investigation can be summarized as follows:

1. The influence of the ablator (heat shield) geometry causes a significant change in trim angle-of-attack and resulting decrease in available lift-to-drag ratio.

2. A very strong viscous influence exists on the Apollo Command Module in the initial portion of re-entry extending down to an altitude of about 220,000 feet.

3. The Mach number influence extends upwards to a value of about 14 which is substantially higher than previous blunt body investigations have indicated.

4. Based on the agreement between wind tunnel data, where real gas effects were not simulated, and both aeroballistic range and full scale flight data, where real gas effects were present, it may be concluded that real gas effects on the static stability of the Apollo Command Module are not significant at velocities up to 27,000 ft/sec.

5. Generally, excellent agreement exists between the Gemini flight test data and data from the AEDC and Langley wind tunnel facilities. The resulting comparison shows how useful a systematic and carefully analyzed wind-tunnel program could be in the prediction of flight aerodynamics of re-entry spacecraft.

ACKNOWLEDGEMENTS

The authors wish to acknowledge contributions to this research work by many of their colleagues at the von Kármán Gas Dynamics Facility (VKF), AEDC. Among the many who assisted in this work, L. K. Ward of the Supersonic Branch (VKF), R. H. Burt of the Hypersonic Branch (VKF), W. R. Lawrence of the Aerophysics Branch (VKF), and W. S. Norman of the Hypervelocity Branch (VKF), contributed materially in obtaining and analyzing the experimental results. The authors are also grateful to Bass Redd and Ralph Graham of the NASA Manned Space Center for providing helpful information and encouragement during the course of the research and to Jack D. Moote of North American Aviation for providing the pertinent details of Apollo Spacecraft 011.

NOMENCLATURE

AWTTP	Apollo Wind Tunnel Test Program
C_A	Axial force coefficient
C_D	Drag force coefficient
C_L	Lift force coefficient
CM	Command Module

$C_{m_{cg}}$	Pitching-moment coefficient referenced to Apollo Mission AS-202 CM center of gravity (see Figs. 6 and 7)
C_N	Normal force coefficient
C_∞	Chapman-Rubesin viscosity coefficient ($\mu_w/\mu_\infty = C_\infty T_w/T_\infty$)
d	Maximum diameter of Apollo or Gemini Command Module (CM)
e	Center of gravity offset from CM centerline (see Figs. 6 and 7)
e/d	Ratio of offset to CM diameter
L/D	Lift-to-drag ratio
M_2	Mach number downstream of a normal shock
M_∞	Free-stream Mach number
p_o'	Pressure, normal shock stagnation conditions
Re_{2d}	Reynolds number downstream of a normal shock based on CM diameter
$Re_{\infty,d}$	Free-stream Reynolds number based on CM diameter
r	Diameter of model sting (see Fig. 5)
T_o'	Temperature, normal shock stagnation conditions
T_w	Wall temperature
T_∞	Free-stream temperature
U_2	Velocity downstream of a normal shock
U_∞	Free-stream velocity
$\bar{v}_\infty$	Viscous interaction parameter defined as $M_\infty(C_\infty/Re_{\infty d})^{1/2}$
X	Distance aft of heat shield (see Figs. 5, 6, and 7)
$X_{c.p.}$	Ratio of longitudinal center of pressure location to CM diameter
$\bar{x}$	Center of gravity location measured longitudinally from aft heat shield (see Figs. 6 and 7)
$\bar{x}/d$	Ratio of longitudinal center of gravity location to CM diameter
Z	Model or spacecraft station (Gemini)
z	Distance normal to centerline of spacecraft (see Fig. 6)
α	Angle of attack, body axis
α_E	Effective angle of attack = $\sqrt{(180 - \alpha)^2 + \beta^2}$
α_T	Trim angle of attack
α'	$180 - \alpha$
β	Angle of sideslip, body axis
γ	Ratio of specific heats
θ	Angle of model sting referenced to centerline of model
θ_b	Local inclination angle of body
λ_2	Mean free path downstream of a normal shock
μ_∞	Free-stream viscosity
μ_2	Viscosity downstream of a normal shock
μ_w	Viscosity based on wall temperature
ρ_∞	Free-stream density

ρ_2 Density downstream of a normal shock

ϕ Reference angle of orientation of Apollo heat shield (see Fig. 3)

σ Shock inclination angle

REFERENCES

1. Moseley, William C., Jr., Moore, Robert H., Jr. and Hughes, Jack E. "Stability characteristics of the Apollo command module," NASA TN D-3890, March 1967.

2. Griffith, B. J. "Comparison of aerodynamic data from the Gemini flights and AEDC-VKF wind tunnels," AIAA J. Spacecraft, Vol. 4, No. 7, pp. 919-924, July 1967.

3. Hillje, Ernest R. "Entry flight aerodynamics from Apollo mission AS-202," NASA TN D-4185, October 1967.

4. Postlaunch Report for Mission AS-201, MSC-A-R-66-4, May 6, 1966.

5. Moseley, William C., Jr. and Martino, Joseph C. "Apollo wind tunnel testing program-historical development of general configurations," NASA TN D-3748, December 1966.

6. Horstmann, C. C. and Kussoy, M. I. "Free-flight measurements of aerodynamic viscous effects on lifting re-entry bodies," AIAA Paper No. 67-165, Presented at the 5th Aerospace Sciences Meeting, January 23, 1967.

7. Whitfield, Jack D. and Griffith, B. J. "Hypersonic viscous drag effects on blunt slender cones," AIAA J., Vol. 2, No. 10, October 1964, pp 1714-1722.

8. Potter, J. Leith "The transitional rarefied-flow regime," Rarefied Gas Dynamics (C. L. Brundin, ed.), Vol. 2, pp. 881-937, Academic Press, New York, 1967.

9. Yos, Jerrold M. "Transport properties of nitrogen, hydrogen, oxygen, and air to 30,000°K," AVCO Report RAD-TM-63-7, March 1963.

10. Lewis, Clark H. and Burgess, E. G., III "Altitude velocity table and charts for imperfect air," AEDC-TDR-64-214 (AD 454078), January 1965.

11. DeRose, Charles E., Ames Research Center, Private communications, December 1967.

12. Seiff, Alvin "Current and future problems in earth and planetary atmosphere entry," AIAA Paper 67-803 (1967).

TABLE 1

POST FLIGHT APOLLO (AS-202)

WIND TUNNEL PROGRAM

(1)	EFFECT OF ASYMMETRY HEAT SHIELD AND SIMULATED PRESSURE PADS	AEDC-VKF Tunnels A,B,C and F M_∞ = 3,4,8,12,15 to 20
(2)	EFFECT OF FLIGHT ANGLE	$\alpha = 180^\circ$ to 150° (All Tunnels)
(3)	MACH NUMBER EFFECTS	M_∞ = 3,4,6,8,10,12,15 to 20
(4)	EFFECT OF REYNOLDS NUMBER	Re_{2d} = 29 to 500,000 (All Tunnels)
(5)	POSSIBLE STING EFFECTS	$M_\infty \sim 8$ AEDC-VKF Range G AEDC-VKF Tunnel B

TABLE 2

NOMINAL TEST FLOW CONDITIONS

a. APOLLO

VKF FACILITY	M_∞	$Re_{\infty d} \times 10^{-3}$	$Re_{2d} \times 10^{-3}$	VKF FACILITY	M_∞	$Re_{\infty d} \times 10^{-3}$	$Re_{2d} \times 10^{-3}$
A	6.0	1900	500	C	12.0	730	55
	4.0	1200	480		12.0	420	30
	3.0	870	470				
				G	6.0	240	80
B	8.0	1800	210		8.5	170	40
	8.0	1000	110		6.0	120	40
	8.0	600	65		8.0	90	20
	8.0	360	40		8.5	50	10
F	14.6	380	21.	L	9.4	1.28	0.16
	19	110	4.7		9.4	0.96	0.12
	20	50	1.8		10.2	0.31	0.04
	18	14	0.68		10.2	0.23	0.03

b. GEMINI

F	15	300	18	L	9.2	1.28	0.15
	19	155	5.4		9.2	0.80	0.10
	20	70	2.4		10.2	0.29	0.32

Langley 11-in. hypersonic (Test Gas - Air)

6.9	360	5

The following page(s) provide higher quality versions of graphics contained in the preceding article or section.

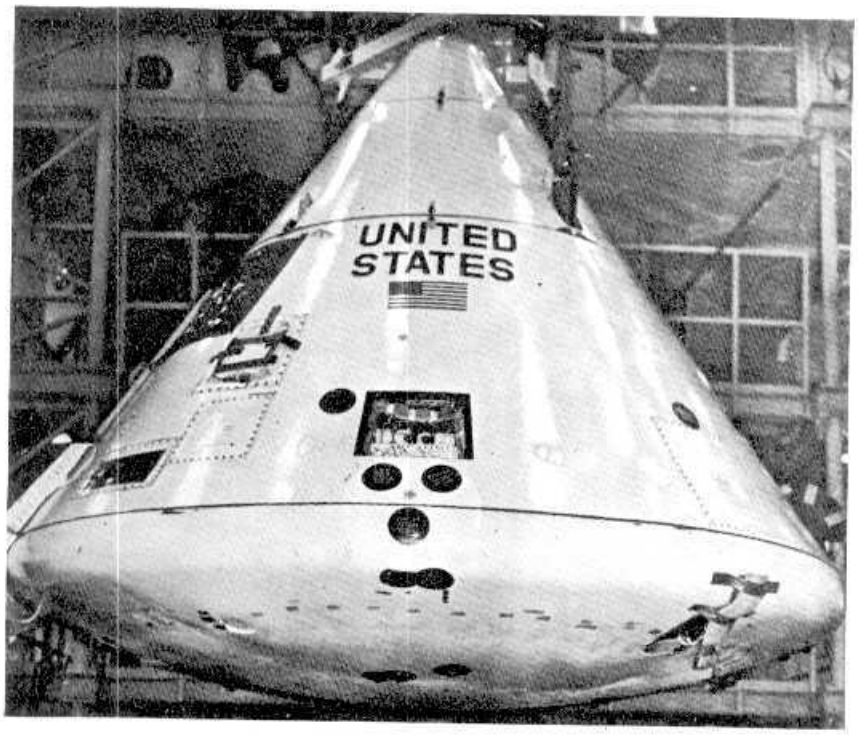

Fig. 1 Photograph of Apollo Spacecraft 011 Prior to Mission AS-202

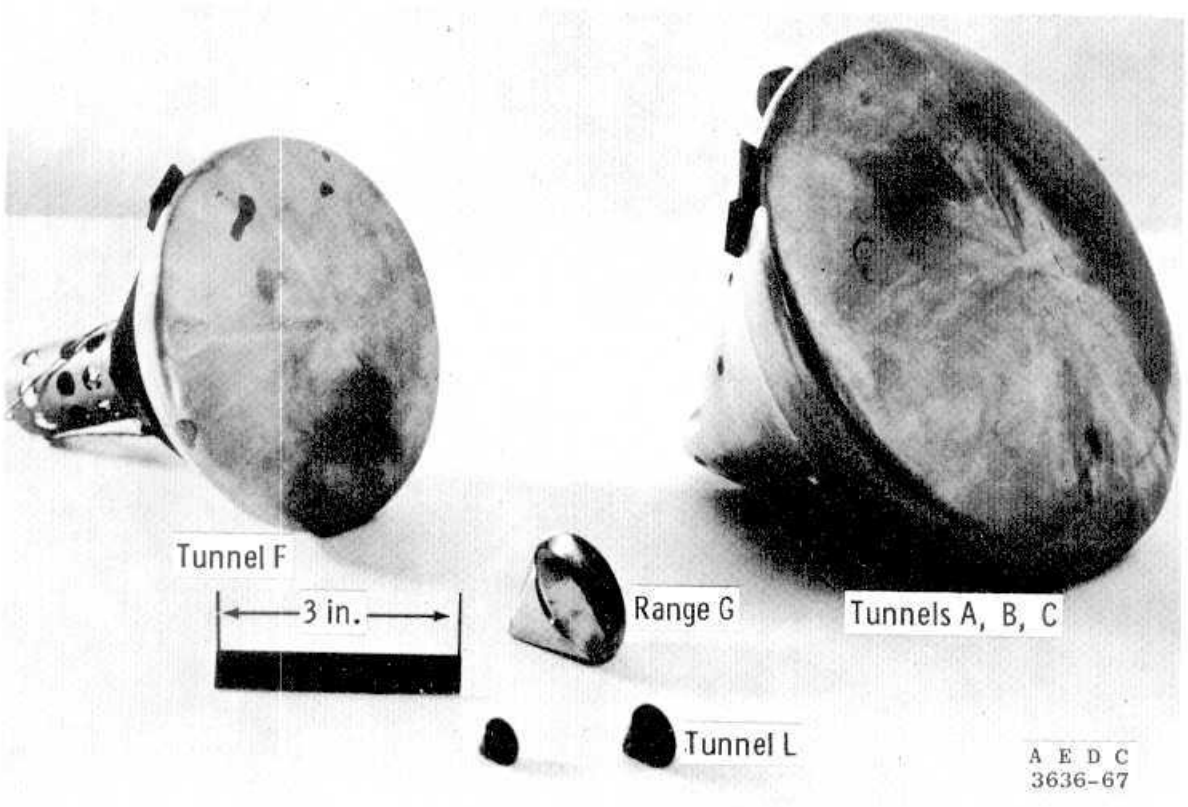

Fig. 2 Photograph of AEDC-VKF Apollo Models

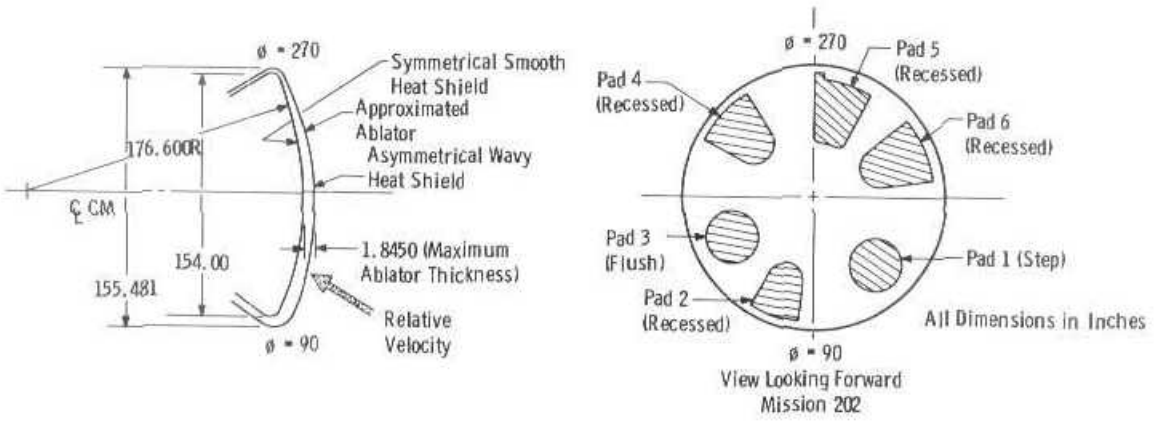

Fig. 3 Apollo 011 Heat Shield Asymmetry

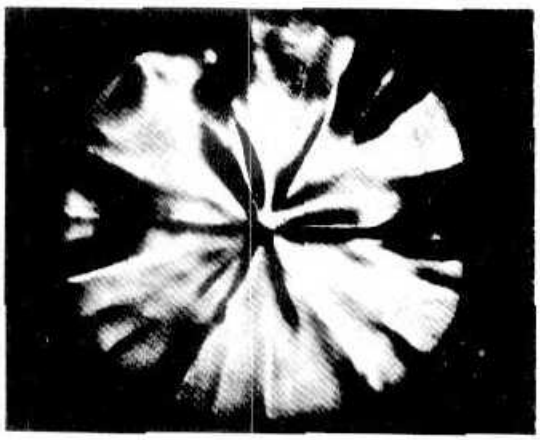

Asymmetrical Wavy Heat Shield

Fig. 4 Optical Photograph of Face of Tunnel F Model

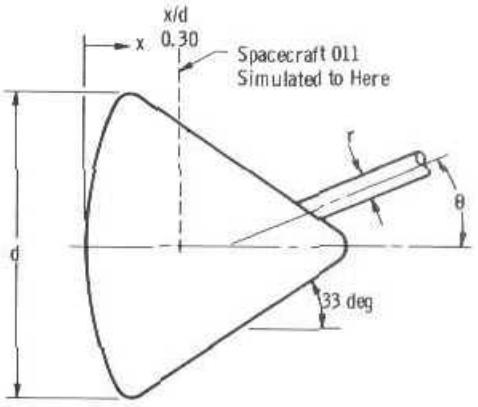

VKF Facility	d	θ, deg	r, in.	Asymmetrical Model
Tunnel A	8.01	20	1.65	Yes
Tunnel B	8.01	20	1.65	Yes
Tunnel C	8.01	20	1.65	Yes
Tunnel F	5.54	0	1.25	Yes
Range G	1.75	-	0	No
Tunnel L	0.60	0	0.16	No
	0.80	0	0.16	No

Fig. 5 Sketch of AEDC-VKF Apollo Models